The Astrophysical Journal Letters, 979:L37 (9pp), 2025 February 01 https://doi.org/10.3847/2041-8213/ada614

A Possible Formation Scenario of the Gaia ID 3425577610762832384: Inner Binary Merger inside a Triple Common Envelope

Zhuowen Li[1], Xizhen Lu[1], Guoliang Lü[1,2], Chunhua Zhu[1], Helei Liu[1], and Jinlong Yu[3]
[1] School of Physical Science and Technology, Xinjiang University, Urumqi, 830046, People's Republic of China; ZhuoWenli2024@163.com, guolianglv@xao.ac.cn, chunhuazhu@sina.cn
[2] Xinjiang Observatory, the Chinese Academy of Sciences, Urumqi, 830011, People's Republic of China
[3] College of Mechanical and Electronic Engineering, Tarim University, Alar, 843300, People's Republic of China
Received 2024 November 28; revised 2025 January 06; accepted 2025 January 06; published 2025 January 28

Abstract

Recently, an identified noninteracting black hole (BH) binary, Gaia ID 3425577610762832384 (hereafter G3425), contains a BH ($\sim 3.6\,M_{\odot}$) falling within the mass gap and has a nearly circular orbit, challenging the classical binary evolution and supernova theory. Here, we propose that G3425 originates from a triple through a triple common envelope (TCE) evolution. The G3425 progenitor originally may consist of three stars with masses of 1.49, 1.05, and 21.81 $M_{\odot}$ and inner and outer orbital periods of 4.22 and 1961.78 days, respectively. As evolution proceeds, the tertiary fills its Roche lobe, leading to a TCE. We find that the orbital energy generated by the inspiral of the inner binary serves as additional energy imparted for ejecting the common envelope (CE), accounting for ∼97% of the binding energy in our calculations. This means that the outer orbit needs to expend only a small amount of the orbital energy to successfully eject the CE. The outcome of the TCE is a binary consisting of a $2.54\,M_{\odot}$ merger produced by the inner binary merger and a $7.67\,M_{\odot}$ helium star whose CE successfully ejected, with an orbital period of 547.53 days. The resulting post-TCE binary (PTB) has an orbital period that is 1–2 orders of magnitude greater than the orbital period of a successfully ejected classical binary CE. In subsequent simulations, we find that the successfully ejected helium star has a 44.2% probability of forming a BH. In the case of a noncomplete fallback forming a BH, with an ejected mass of $2.6\,M_{\odot}$ and a relatively low natal kick (11^{+16}_{-5} km s^{-1} to 49^{+39}_{-39} km s^{-1}), this PTB can form G3425 in the Milky Way.

Unified Astronomy Thesaurus concepts: Black holes (162)

1. Introduction

Black hole (BH) binaries are excellent laboratories for understanding massive star evolution, binary evolution, and supernovae (SNe). So far, most observed BH binaries are BH X-ray binaries (J. E. McClintock & R. A. Remillard 2006; R. A. Remillard & J. E. McClintock 2006; J. Casares & P. G. Jonker 2014; J. M. Corral-Santana et al. 2016), which are also the most studied type of BH binaries (e.g., K. Belczynski & J. Ziolkowski 2009; Y. Shao & X.-D. Li 2015; M. U. Kruckow et al. 2018; M. Mapelli & N. Giacobbo 2018; and Y. Shao & X.-D. Li 2020). However, based on the observed outburst characteristics and distance distribution of known BH X-ray binaries, their number is expected to represent only a small fraction of the entire BH binary population (J. M. Corral-Santana et al. 2016).

With the rapid advancement of astrometric instruments and technology, noninteracting BH binaries are also gradually being unveiled. Very recently, Gaia DR3, the prerelease of Gaia DR4, LAMOST, and Gaia DR2 have confirmed four noninteracting BH binaries using spectroscopic and astrometric data, named Gaia BH1 (S. Chakrabarti et al. 2023; K. El-Badry et al. 2023b), Gaia BH2 (K. El-Badry et al. 2023a; A. Tanikawa et al. 2023), Gaia BH3 (Gaia Collaboration et al. 2024), and Gaia ID 3425577610762832384 (hereafter G3425; S. Wang et al. 2024). G3425 has many unique features, and some of its physical properties are listed in Table 1. Compared to known BH X-ray binaries, G3425 has a much longer orbital period. Additionally, the BH in G3425 has a much lower mass compared to the BHs in Gaia BH1, Gaia BH2, and Gaia BH3, falling within the $3 \sim 5\,M_{\odot}$ range. BHs within this mass range are rare in known BH binaries, the range often referred to as the mass gap (C. D. Bailyn et al. 1997; C. L. Fryer & V. Kalogera 2001; D. Özel et al. 2010; W. M. Farr et al. 2011). Furthermore, G3425 has a lower eccentricity compared to Gaia BH1, Gaia BH2, and Gaia BH3, with its orbit being closer to circular.

G3425 challenges the classical binary evolution theory. In the discussion of the isolated binary origin of G3425 by S. Wang et al. (2024), they consider the high mass ratio between the BH progenitor and the visible giant in G3425. If the progenitor binary underwent mass transfer (MT), it is likely that it went through the common envelope evolution (CEE) phase. In the CEE simulations by S. Wang et al. (2024), forming G3425 typically requires an excessively large ejection efficiency parameter ($\alpha_{\rm CE}$), with typical $\alpha_{\rm CE}$ values ranging from $5 \sim 10$. Recently, A. Gilkis & T. Mazeh (2024) and M. U. Kruckow et al. (2024) proposed that increasing the overshooting parameter or stellar wind strength in massive stars could suppress the expansion of their radii, potentially allowing the progenitor binary of G3425 to avoid undergoing Roche lobe overflow (RLOF). However, in the simulations by S. Wang et al. (2024), even with a tenfold increase in stellar wind strength, the progenitor of this BH still fills its Roche lobe radius. On the other hand, in the analysis by S. Wang et al. (2024), G3425 is suggested to possibly originate from a triple, where the BH is formed from the merger of two neutron stars (NSs) or a Thorne–Żytkow object (the product of the merger of a NS with a giant star; P. Podsiadlowski et al. 1995). However, in the triple population synthesis analysis by J. Stegmann et al. (2022), no surviving triples were found with an inner binary

Table 1
Physical Parameters of the Observed G3425

Physical Parameter	G3425
$M_{\rm RG}$ ($M_\odot$)	$2.66^{+1.18}_{-0.68}$
$M_{\rm BH}$ ($M_\odot$)	$3.6^{+0.8}_{-0.5}$
$P_{\rm orb}$ (days)	877^{+2}_{-2}
e	$0.05^{+0.01}_{-0.01}$
[Fe/H]	$-0.12^{+0.02}_{-0.02}$
$R_{\rm RG}/R_{\rm RG,L}$	∼4.5%

Note. The second and third rows provide the masses of the optical companion and BH, respectively. The optical companion is an RG star. Rows four and five show the orbital period and eccentricity, respectively. The sixth row and the last row represent the metallicity and the ratio of the RG's radius to its Roche lobe radius, respectively. The data come from S. Wang et al. (2024).

consisting of a binary NS, unless it is assumed that there were zero natal kicks during the formation of the NS.

It is well known that a high fraction of massive stars are born in triple or multiple stars (H. Sana et al. 2013; M. Moe & R. Di Stefano 2017). Based on the observational statistics of M. Moe & R. Di Stefano (2017), more than ∼70% of massive stars are in triple or higher-order (e.g., quadruple) configurations. Hierarchical triples are known for their long-term von Zeipel–Lidov–Kozai (ZLK) oscillations, which are caused by the exchange of angular momentum between the inner and outer orbits (H. von Zeipel 1910; Y. Kozai 1962; M. L. Lidov 1962; S. Naoz 2016). This leads to the excitation of the eccentricity and inclination of the inner orbit, which ultimately enhances tidal effects, gravitational wave emission, and inner binary interactions (e.g., MT and collisions; S. Naoz & D. C. Fabrycky 2014; S. Toonen et al. 2016; S. Naoz et al. 2016; J. M. Salas et al. 2019; S. Toonen et al. 2020; C. Shariat et al. 2023; C. W. Bruenech et al. 2025). Recent studies also suggest that the ZLK mechanism in triples can explain the origin of events such as low-mass X-ray binaries (LMXBs; S. Naoz et al. 2016; C. Shariat et al. 2024), high-velocity runaway stars (J. M. Salas et al. 2019; C. W. Bruenech et al. 2025), Type Ia SNe (S. Toonen et al. 2018a; A. S. Rajamuthukumar et al. 2023; C. Shariat et al. 2023), blue straggler binaries (S. Naoz & D. C. Fabrycky 2014; C. Shariat et al. 2025), NS and white dwarf merger (S. Toonen et al. 2018b), and binary BH mergers (F. Antonini et al. 2017; M. A. S. Martinez et al. 2020). In addition, the interaction of triple RLOF in hierarchical triples has gained increasing attention (N. de Vries et al. 2014; T. A. F. Comerford & R. G. Izzard 2020; H. Glanz & H. B. Perets 2021; A. S. Hamers et al. 2022a; A. S. Rajamuthukumar et al. 2023; K. B. Burdge et al. 2024; F. Kummer et al. 2025). During this phase, the tertiary overflows its Roche lobe, transferring mass to the inner binary. Triple RLOF can lead to either stable or unstable MT. In the case of unstable MT, it can result in a triple common envelope (TCE), where the extended envelope engulfs the inner binary and the core of the tertiary. During the TCE process, the inner binary inspiral each other and toward the core of the donor due to friction (N. Ivanova et al. 2013; N. Ivanova et al. 2020; F. K. Röpke & O. De Marco 2023). TCE can result in various possible outcomes, such as the merger of the inner binary, the ejection of one star (usually the least massive component), and chaotic triple dynamics, among others (E. Sabach & N. Soker 2015; T. A. F. Comerford & R. G. Izzard 2020; H. Glanz & H. B. Perets 2021; N. Soker 2021; A. S. Hamers et al. 2022a; C. W. Bruenech et al. 2025). Here, we propose that G3425 may originate from a hierarchical triple that underwent TCE. In this scenario, the tertiary is the progenitor of the BH, while the giant evolved from the merger product of the inner binary. If the contribution of the orbital energy of the inner binary to common envelope (CE) ejection is considered during the TCE process, the outer orbit may not require excessive energy to successfully eject CE. In other words, the outer orbit does not need to spiral in as deeply as in a binary CEE. Typically, in a binary CEE process, for $\alpha_{\rm CE}=1$, the post-CEE orbital period is $<\sim$10 days (N. Ivanova et al. 2013; N. Ivanova et al. 2020; F. K. Röpke & O. De Marco 2023). The results suggest that the post-TCE binary (PTB) may have longer orbital period, which potentially could explain G3425.

The structure of this Letter is as follows. In Section 2, we describe the modeling of the evolution of the progenitor triple of G3425, the TCE process, the evolution of the PTB, and the modeling of SNe. In Section 3, we present the computational results for the formation of G3425, followed by a conclusion in Section 4.

2. Methodology

The formation of G3425 in our simulation is divided into several subprocesses. It starts with the evolution of the initial triple until the TCE occurs, then the modeling of the TCE process and the evolution of the PTB, and finally the occurrence of SNe and the evolution of the post-SNe binary (up to Hubble time). In the following subsections, we explain the modeling methods of these subprocesses in detail.

2.1. Modeling of Triple Evolution and TCE

Following A. S. Hamers et al. (2021), A. S. Hamers et al. (2022b), and Z. Li et al. (2024b), we require the initial triple to be dynamically stable. Specifically, we require the initial triple to satisfy the formula from R. A. Mardling & S. J. Aarseth (2001), which is

$$\frac{a_{\rm out}}{a_{\rm in}} > 2.8\left(1+\frac{m_3}{m_1+m_2}\right)^{\frac{2}{5}}\frac{(1+e_{\rm out})^{\frac{2}{5}}}{(1-e_{\rm out})^{\frac{6}{5}}}\left(1-\frac{0.3i}{180^\circ}\right). \quad (1)$$

Here, for a hierarchical triple, two stars are on a tighter orbit (the inner binary), while the third companion orbits the inner binary on a wider orbit (i.e., the center of mass of the inner binary and the tertiary form an outer binary). The subscripts "in" and "out" denote the inner and outer parts of the triple, respectively. Subscripts 1, 2, and 3 refer to the primary, the secondary in the inner binary, and third component, respectively. The symbol i represents the mutual inclination between the pairs of orbits. Additionally, we reject initial inner binaries that are in RLOF at periastron by using P. P. Eggleton's (1983) analytical formula to calculate the Roche lobe radius and $R_{\rm ini}=R_\odot(m_{\rm ini}/M_\odot)^{0.7}$ (R. Kippenhahn & A. Weigert 1994) to estimate the initial stellar radius. For the initial triples that meet the above criteria, we use the Multiple Stellar Evolution (MSE) code (A. S. Hamers et al. 2021) to simulate their evolution. The advantage of the MSE code is that it includes rapid fitting formulas for single-star evolution (J. R. Hurley et al. 2000), binary interactions (e.g., tidal effects, MT; J. R. Hurley et al. 2002), flybys, and dynamical perturbations in multiple systems. For the long-term dynamical evolution of multiple systems, the MSE code uses orbital-

averaged integration when the system is sufficiently hierarchical (A. S. Hamers & S. F. Portegies Zwart 2016; A. S. Hamers 2018, 2020) and self-consistent modeling through n-body methods when the system is dynamically unstable (A. Rantala et al. 2020). However, the MSE code still has certain limitations. For example, the rapid fitting formulas for single-star evolution and binary interactions included in the MSE code are extreme approximations. In some cases, they may overshoot the radius evolution of single stars and make approximations during MT evolution. Additionally, these rapid fitting formulas do not model stellar structure. Considering the high metallicity of the visible companion of G3425, the triple is set with a typical Galactic metallicity of $Z = 0.014$ (C. Ekström et al. 2012). Moreover, for parameter values in the MSE code that are not mentioned in this Letter, we use the default values.

When the tertiary fills its Roche lobe and MT occurs, we follow the default settings of the MSE code, using the critical mass ratio to determine whether the MT is stable. If the MT is unstable, it will lead to TCE. However, the evolution of TCE is still highly uncertain, as it often requires detailed modeling involving higher dimensions, such as hydrodynamics and gravitational dynamics (E. Sabach & N. Soker 2015; T. A. F. Comerford & R. G. Izzard 2020; H. Glanz & H. B. Perets 2021; N. Soker 2021; A. S. Hamers et al. 2022a). In one of the 3D numerical simulation results by H. Glanz & H. B. Perets (2021) on TCE, both the inner and outer orbits undergo inspiral due to friction, and their orbital energy changes ($\Delta E_{\rm orb}$) contribute to the ejection of the CE. Therefore, we use the standard energy prescription to first assume that both the inner and outer orbital energies contribute to the consumption of the binding energy ($E_{\rm bind}$). The specific formula is as follows (B. Paczynski 1976; E. P. J. van den Heuvel 1976; R. F. Webbink 1984; M. Livio & N. Soker 1988; J. Iben & M. Livio 1993; N. Ivanova et al. 2013):

$$E_{\rm bind} = \alpha_{\rm CE,in}\Delta E_{\rm orb,in} + \alpha_{\rm CE,out}\Delta E_{\rm orb,out}. \quad (2)$$

Here, $E_{\rm bind}$ of the envelope is contributed by the envelope of the tertiary. The changes in inner orbital energy $\Delta E_{\rm orb,in}$ and outer orbital energy $\Delta E_{\rm orb,out}$ are calculated as the differences between the orbital energies before and after the inspiral, respectively, as follows:

$$\begin{cases} E_{\rm bind} = G\dfrac{m_3 m_{3,\rm env}}{\lambda R_3} \\ \Delta E_{\rm orb,in} = -\dfrac{Gm_1 m_2}{2a_{\rm in,i}} + \dfrac{Gm_1 m_2}{2a_{\rm in,f}} \\ \Delta E_{\rm orb,out} = -\dfrac{Gm_3(m_1+m_2)}{2a_{\rm out,i}} + \dfrac{Gm_{3,\rm core}(m_1+m_2)}{2a_{\rm out,f}}. \end{cases} \quad (3)$$

Here, G represents the gravitational constant. Subscripts i and f denote the states before and after the inspiral, respectively, while subscripts env and core refer to the envelope (hydrogen-rich envelope) and core (helium core) of the donor star (here, the tertiary). The parameters $\alpha_{\rm CE,in}$ and $\alpha_{\rm CE,out}$ represent the ejection efficiency for the inner and outer orbital energies, respectively. Based on the general settings used in many previous population synthesis calculations (e.g., N. Giacobbo et al. 2018, Y. Shao & X.-D. Li 2020, Y. Shao & X.-D. Li 2021, C. Chawla et al. 2022, and C. Chawla et al. 2024), we set $\alpha_{\rm CE,in} = \alpha_{\rm CE,out} = 1$. Although $\alpha_{\rm CE}$ is very important in TCE evolution, with larger values making it easier to eject CE during the TCE process (H. Glanz & H. B. Perets 2021), it remains highly uncertain (M. Zorotovic et al. 2010; N. Ivanova et al. 2013; F. K. Röpke & O. De Marco 2023). Recent numerical simulations of CEE suggest that $\alpha_{\rm CE}$ may range from 0.5 to 2.12 (M. Vetter et al. 2024). λ represents the structural parameters of the envelope, for which we use a typical value of $\sim$0.1 for massive stars (X.-J. Xu & X.-D. Li 2010; A. J. Loveridge et al. 2011; N. Giacobbo et al. 2018). Additionally, in one of the simulation results from the study by H. Glanz & H. B. Perets (2021), the inner binary inspirals faster than the outer binary. Therefore, we also assume that during the TCE process, $a_{\rm in}$ decreases faster than $a_{\rm out}$ ($a_{\rm in}/a_{\rm out}$ keeps decreasing and satisfying Equation (1)). This ensures that the triple remains dynamically stable during TCE and that $E_{\rm bind}$ is always consumed first by the inner orbital energy ($E_{\rm orb,in}$), followed by the outer orbital energy ($E_{\rm orb,out}$). Under the above assumptions, using the standard energy prescription, we estimate the following possible outcomes of TCE (N. Ivanova et al. 2013; H. Glanz & H. B. Perets 2021; F. K. Röpke & O. De Marco 2023):

(i) If $E_{\rm bind} < \Delta E_{\rm orb,in}$, during the TCE process, the CE is ejected, and the inner binary combines with the helium star (the core of the tertiary) to form a new triple.
(ii) If $\Delta E_{\rm orb,in} < E_{\rm bind} < \Delta E_{\rm orb,in} + \Delta E_{\rm orb,out}$, during the TCE process, the CE is ejected, but the inner binary merges, and the merger product of the inner binary combines with the helium star (the core of the tertiary) to form a binary.
(iii) If $E_{\rm bind} > \Delta E_{\rm orb,in} + \Delta E_{\rm orb,out}$, during the TCE process, the CE is not completely ejected. The inner binary merges, and its merger product also merges with the helium star (the core of the tertiary). As a result, the TCE leads to a single star.

We adopt the assumption of J. R. Hurley et al. (2002), J. J. Eldridge et al. (2017), N. Giacobbo et al. (2018), A. S. Hamers et al. (2021), J. Riley et al. (2022), and Z. Li et al. (2024a, 2024b) that when $a_{\rm in,f} = R_1 + R_2$, the two stars merge. Additionally, following C. A. Tout et al. (1997) and J. R. Hurley et al. (2002), we assume when two main-sequence (MS) stars merge, their material is fully mixed, and the merger product remains an MS star. We also assume no mass loss during the merger process, meaning the mass of the merger product is $M_{\rm mer} = m_1 + m_2$ (C. A. Tout et al. 1997; J. R. Hurley et al. 2002). We emphasize that this approach remains highly simplified, but it does capture some of the key results from the TCE simulations by H. Glanz & H. B. Perets (2021).

2.2. Modeling of Post-TCE and SNe

Using the methods described in the previous section, we calculate the possible outcomes of TCE. In scenarios where the inner binary merges and the outer binary successfully ejects CE, the merger product of the inner binary and the core of the tertiary (a helium star) form the PTB. For the PTB, we use MESA stellar evolution code (B. Paxton et al. 2011, 2013, 2015, 2018, 2019; version 10398) to track its evolution. Similar to X. Lu et al. (2023) and Y. Qin et al. (2023), we use the MESA code to create helium-rich stars and then relax the created helium star until the ratio of its helium-burning luminosity to total luminosity exceeds 99%. We apply the Ledoux criterion and the standard mixing-length theory

($\alpha_{\rm MLT} = 1.5$) for convection calculations (N. Langer 1991). The overshooting parameter is set to 0.335 (I. Brott et al. 2011), and the semiconvection parameter is 1 (N. Langer 1991). For helium-rich stars, its stellar wind scheme is adopted by T. Nugis & H. J. G. L. M. Lamers (2000).

Following D. Pauli et al. (2022), X. Lu et al. (2023), and T. Fragos et al. (2023), when the helium star evolves to the point of core carbon depletion, we assume it undergoes an SN. To date, SNe still involve significant uncertainties (C. L. Fryer et al. 2012; B. Müller et al. 2016; I. Mandel & B. Müller 2020; F. R. N. Schneider et al. 2021). For the type and mass of the remnant after an SN, we use the semianalytical model of I. Mandel & B. Müller (2020) for simulation. Specifically, we first determine the remnant probability distribution based on the carbon–oxygen core mass ($M_{\rm CO}$), and the detailed analytical formula is as follows (I. Mandel & B. Müller 2020):

$$\begin{cases} P_{\rm NS} = 1, & \text{if} \quad M_{\rm CO} < 2M_\odot \\ P_{\rm BH} = \dfrac{M_{\rm CO} - 2}{5} \text{and} P_{\rm NS} \\ \quad = 1 - P_{\rm BH}, & \text{if} 2M_\odot \leqslant M_{\rm CO} < 7M_\odot \\ P_{\rm BH} = 1, & \text{if} \quad M_{\rm CO} \geqslant 7M_\odot \end{cases}. \tag{4}$$

Second, if the remnant is a BH, we calculate the probability of it forming through complete fallback (CF), and the specific formula is as follows (I. Mandel & B. Müller 2020):

$$\begin{cases} P_{\rm CF} = 1, & \text{if} \quad M_{\rm CO} \geqslant 8M_\odot \\ P_{\rm CF} = \frac{M_{\rm CO} - 2}{6}, & \text{if} \quad 2M_\odot \leqslant M_{\rm CO} \leqslant 8M_\odot \end{cases} \tag{5}$$

If BH is formed through CF, its mass equals the mass of the helium core (helium stars). Otherwise, its mass is drawn from a normal distribution with a mean of $0.8M_{\rm CO}$ and a standard deviation of 0.5 (I. Mandel & B. Müller 2020). We also set the minimum BH mass to $2\,M_\odot$. If the generated BH mass falls below this limit, we redraw it until it falls within the allowed range. Nevertheless, we emphasize that our method has certain uncertainties. In the catalog of BH transients of J. M. Corral-Santana et al. (2016), the BH mass function remains uncertain. Furthermore, in the study by T. Sukhbold et al. (2016), if the pre-SN star undergoes only helium core collapse, the average BH mass is in the range of $7.7 \sim 9.2\,M_\odot$, and it is predicted that BH cannot form in the mass gap ($3 \sim 5\,M_\odot$). On the other hand, observational evidence for BH natal kicks remains quite limited (K. B. Burdge et al. 2024). Many previous studies suggest that the natal kicks received by BH can be large (tens to hundreds of $\rm km\,s^{-1}$; J. J. Andrews & V. Kalogera 2022; M. S. B. Coleman & A. Burrows 2022; A. Burrows et al. 2023; C. Kimball et al. 2023; D. Mata Sanchez et al. 2024), but they can also be very small ($<10\,\rm km\,s^{-1}$; L. Walk et al. 2020; K. De et al. 2024; H.-T. Janka & D. Kresse 2024; P. Nagarajan & K. El-Badry 2024; A. Rostami-Shirazi et al. 2024; R. Willcox & I. Tamborra 2024) or even zero (I. F. Mirabel & I. Rodrigues 2003; T. Shenar et al. 2022). In previous research, low natal kicks ($<40 \sim 50\,\rm km\,s^{-1}$) are preferred for wide-orbit BH binaries like Gaia BH1 and Gaia BH2 (K. El-Badry et al. 2023b, 2023a; I. Kotko et al. 2024; Z. Li et al. 2024b). Additionally, very recently, in some observed triples containing a BH (e.g., V404 Cygni), the natal kicks of this BH at formation were almost negligible ($<5\,\rm km\,s^{-1}$; K. B. Burdge et al. 2024; C. Shariat et al. 2024). Therefore, we assume natal kicks are drawn from Maxwellian distributions with dispersions ($\sigma_{\rm k}$) of 10 and $50\,\rm km\,s^{-1}$, respectively. However, in some previous studies, the distribution of kicks is sometimes considered to depend on the mass of the BH (C. L. Fryer et al. 2012). This means that low-mass BH would receive significant kicks, making it harder for the binary to survive. Therefore, using only Maxwellian distributions with $\sigma_{\rm k}$ of 10 and 50 $\rm km\,s^{-1}$ to describe the kick distribution in this Letter may underestimate the kick velocity for low-mass BH. For these two scenarios, we draw 5×10^6 repetitions of the type of the remnant, the mass of the remnant, orientation angle of SNe, mean anomaly of SNe, and natal kick as a way to investigate whether PTBs can form G3425 during the SNe process. Finally, we use the Binary Star Evolution code (J. R. Hurley et al. 2002) to track the evolution of the post-SNe binary up to Hubble time.

3. Results

Studying the formation of G3425 through TCE is crucial for understanding the evolution of massive stars, the evolution of triples, the CEE, and the SNe. In the following subsection, we present the detailed computational results for the formation of G3425.

3.1. Formation of G3425

Following Z. Li et al. (2024b), we use Monte Carlo simulations to generate the initial input parameters of triples. In the Monte Carlo simulations, we mainly consider both the results of the 3D simulations of TCE by H. Glanz & H. B. Perets (2021) and the observed characteristics of G3425. Under the assumption that G3425 can form through the merger of the inner binary in the TCE process, we constrain the mass range as $2.5\,M_\odot < m_{1,\rm ini} + m_{2,\rm ini} < 2.7\,M_\odot$, which roughly corresponds to the mass of the visible companions of G3425. Additionally, according to the discussion by S. Wang et al. (2024), the BH mass that forms G3425 is estimated to require a helium core mass before the SN between 5 and $7\,M_\odot$. Therefore, we constrain the mass range as $21\,M_\odot < m_{3,\rm ini} < 22\,M_\odot$. On the other hand, the results of the 3D simulations of TCE by H. Glanz & H. B. Perets (2021) show that, during the TCE process, the inner binary can only inspiral faster than the outer binary if the orbital separation is relatively small (about $3 \sim 26\,R_\odot$ in their simulations). Therefore, we constrain the range as $5\,R_\odot < a_{\rm in,ini} < 20\,R_\odot$. For the outer orbit, considering the possibility that the tertiary can fill its Roche lobe (with the maximum radius of about $1000 \sim 4000\,R_\odot$), we constrain $a_{\rm out,ini} < 15$ au. Combining this with the stability criterion for the initial triple, we perform Monte Carlo simulations within these ranges to search for orbits that resemble the formation of G3425. We select an initially dynamically stable triple, which undergoes TCE to evolve into a PTB and eventually forms G3425 after a SN event. The initial masses of the three stars in the triple system are 1.49, 1.05, and $21.81\,M_\odot$; the inner and outer orbital periods are 4.22 and 1961.78 days, respectively; and the inner and outer eccentricities are 0.08 and 0.15, respectively. Additionally, the inner and outer inclinations (radians) are 1.73 and 1.27, respectively; the inner and outer arguments of pericenter (radians) are 4.68 and 3.61, respectively; and the inner and outer longitudes of ascending node (radians) are 4.35 and 0.61, respectively.

In Figures 1 and 2, we show the motion diagram at key points during the evolution of the selected triple and the functions of orbital period, eccentricity, mass, and radius over time,

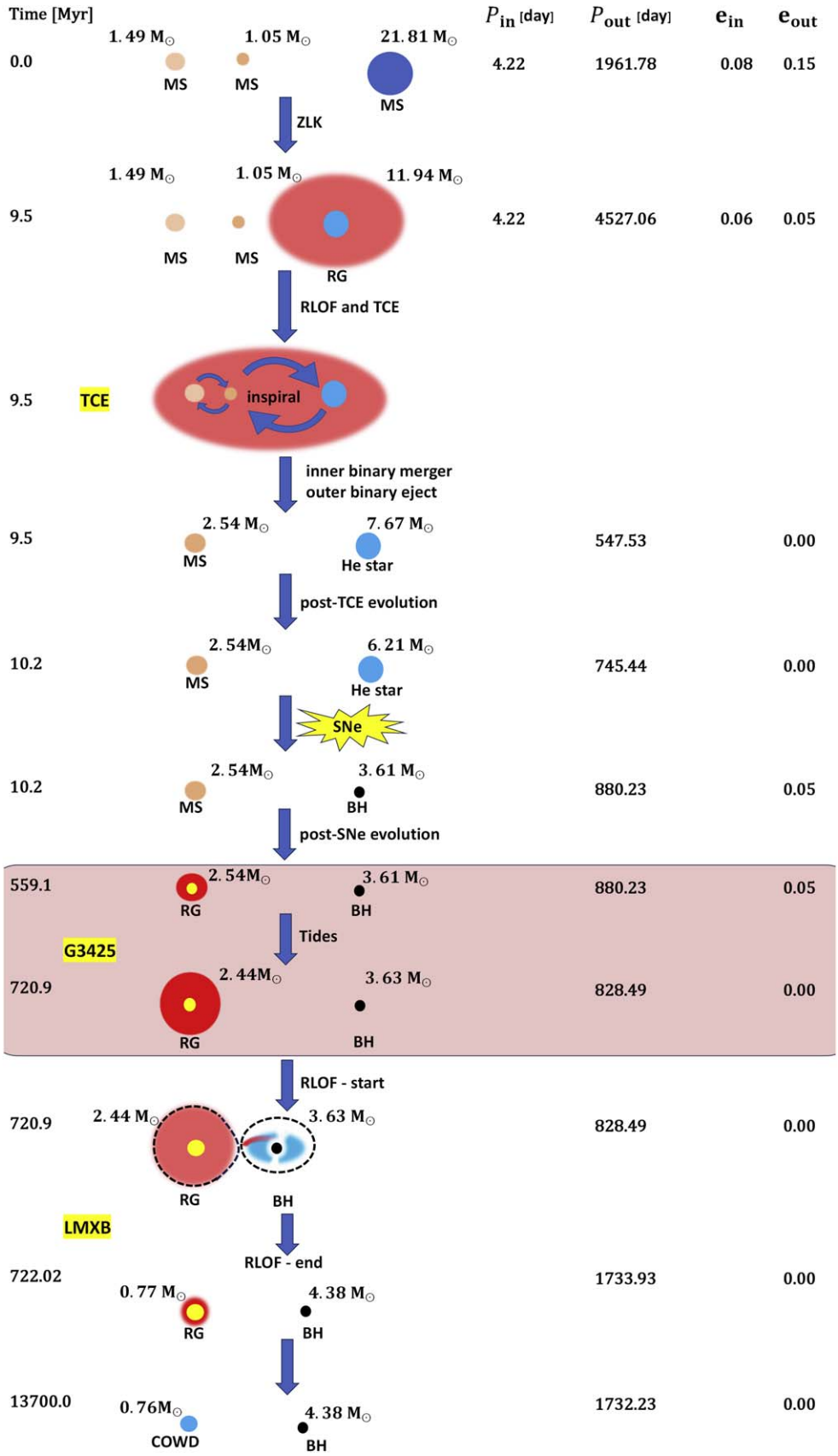

Figure 1. The key evolutionary stage diagram of the initial triple leading to the formation of G3425, where the light-red shaded area represents the duration of the observed G3425 phase.

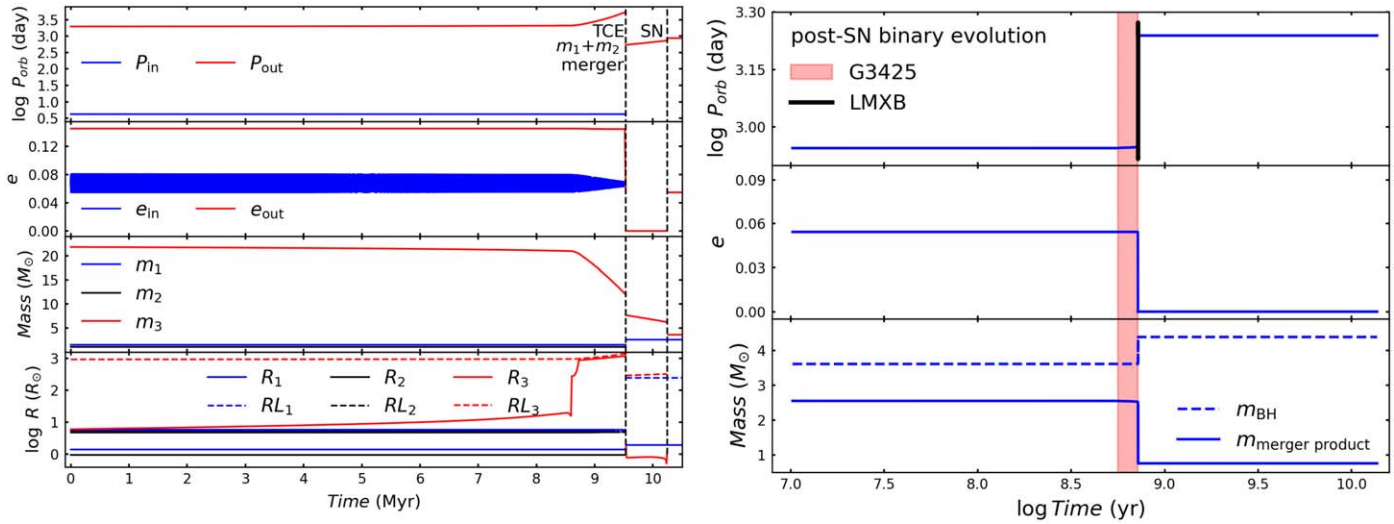

Figure 2. The time functions of orbital period (P_{orb}), eccentricity (e), mass, and radius for the selected triple.

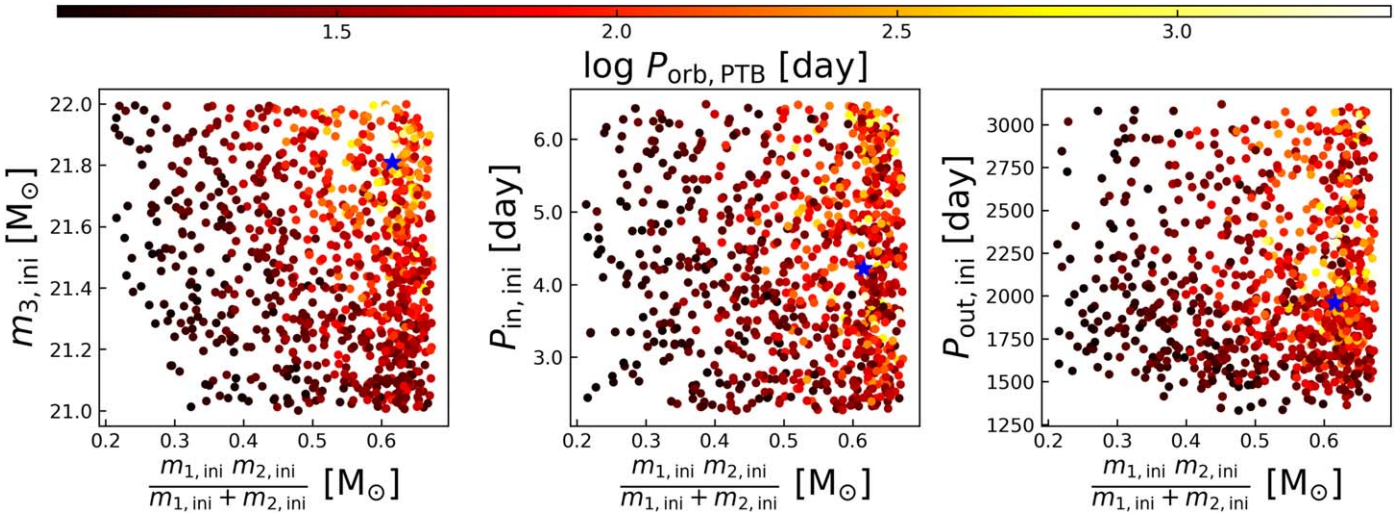

Figure 3. The distribution of the initial reduced mass of the inner binary ($\frac{m_{1,ini}m_{2,ini}}{m_{1,ini}+m_{2,ini}}$), the initial mass of the tertiary, the initial inner and outer orbital periods, and the orbital period of the PTBs ($P_{PTB,orb}$) under the assumption that $\alpha_{CE,in} = \alpha_{CE,out} = 1$. Different colors represent the orbital periods of the PTBs, with the blue stars indicating the initial parameters selected in Figures 1 and 2.

respectively. In this triple, the tertiary has the greatest mass, evolves at the fastest rate, and its Roche lobe around the inner binary ($\sim 925\,R_\odot$). As the tertiary evolves, its radius begins to expand, and the outer orbital period evolves through adiabatic expansion due to mass loss from stellar winds, with e_{out}, remaining nearly unchanged (J. R. Hurley et al. 2002). On the other hand, the ZLK effect, triggered by the exchange of angular momentum between the inner and outer orbits, causes e_{in} to undergo long-term oscillations (H. von Zeipel 1910; Y. Kozai 1962; M. L. Lidov 1962; S. Naoz 2016) within the range of $0.05 \sim 0.08$. At $\sim$8.6 Myr, the tertiary leaves the MS stage, quickly passes through the Hertzsprung gap, and enters the red giant (RG) phase. During this time, its radius rapidly expands, and a large amount of mass is lost through RG stellar winds. This results in a rapid increase in the P_{out} and strengthens the tidal (J. R. Hurley et al. 2002). The ZLK effect is suppressed by the short-range tidal forces, leading to a gradual reduction in the oscillation amplitude (M. Holman et al. 1997; P. P. Eggleton & L. Kiseleva-Eggleton 2001; O. Blaes et al. 2002; K. R. Anderson et al. 2017; A. Dorozsmai et al. 2024). At $\sim$9.5 Myr, the tertiary undergoes RLOF, with $P_{in} = 4$ days ($a_{in} = 15\ R_\odot$), $P_{out} = 4527$ days ($a_{out} = 2807\ R_\odot$), $m_3 = 11.94\,M_\odot$ ($m_{3,c} = 7.67\,M_\odot$ and $m_{3,env} = 4.27\,M_\odot$), and $(m_1 + m_2) = 2.54\,M_\odot$. Due to the very large mass ratio ($q = m_3/(m_1 + m_2) = 4.7$), the MSE code determines that the MT is unstable, and the triple enters the TCE phase.

Based on the simulations by H. Glanz & H. B. Perets (2021) and the modeling in Section 2.2, we assume that the inner binary merges due to inspiral during the TCE phase. Combining Equations (2) and (3), we calculate the E_{bind} to be 3.75×10^{48} erg and the separation of the inner binary from $15\,R_\odot$ of separation before inspiral to $(R_1 + R_2) \cong 2.34\ R_\odot$ when the merger occurs after inspiral produces $\sim 3.68 \times 10^{48}$ erg of $E_{orb,in}$, which is about 97% of the E_{bind}. This means that, in order to successfully eject CE, the remaining 3% of the E_{bind} needs to be provided by the $E_{orb,out}$. Under this assumption of $\alpha_{CE,in} = \alpha_{CE,out} = 1$, we calculate that the a_{out} only needs to inspiral from its initial value of 2807 to 687 $R_\odot$ to successfully eject CE. It is worth noting that if a larger $\alpha_{CE,in}$ or/ and $\alpha_{CE,out}$ is assumed when the inner binary merges, we

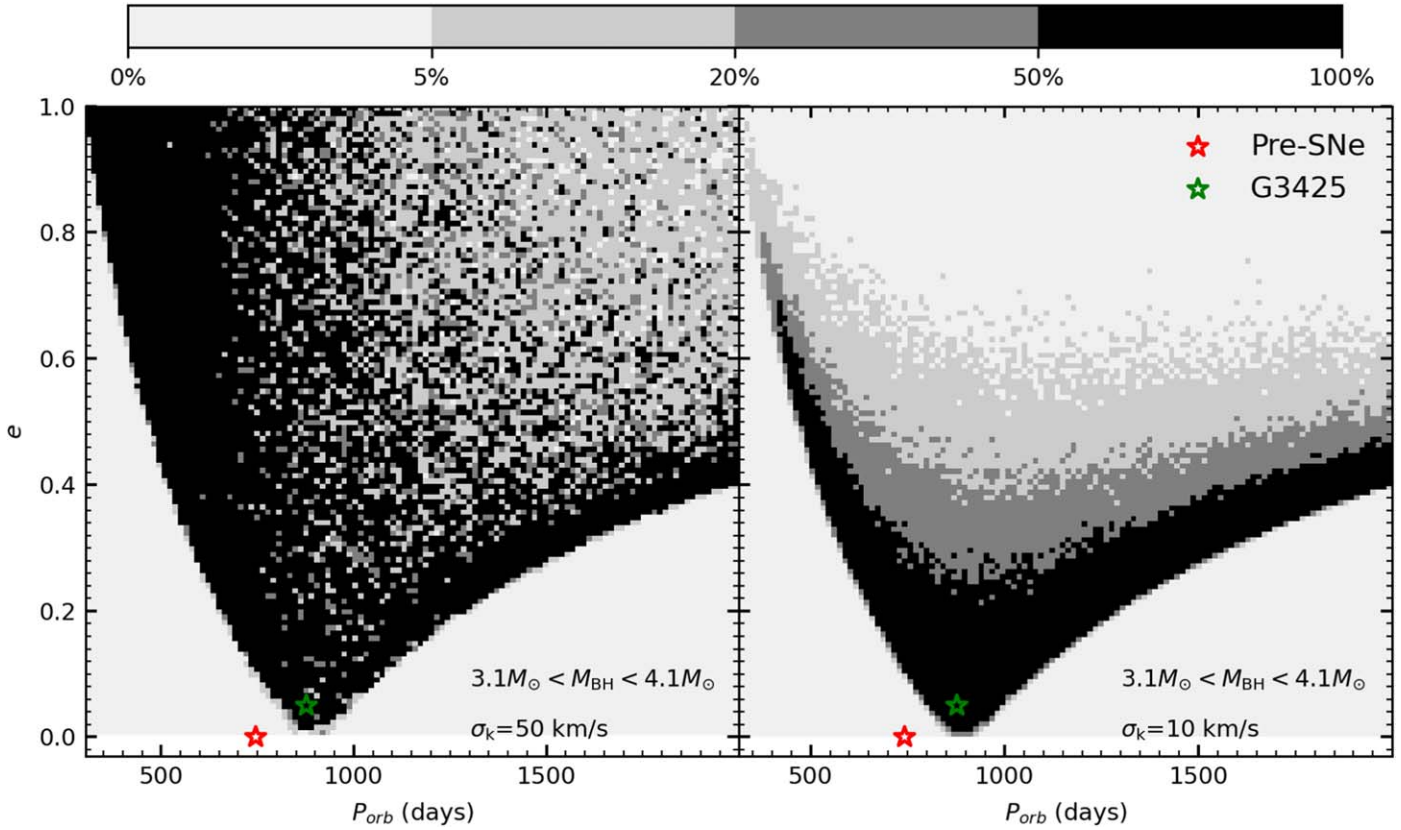

Figure 4. The probability distribution of the orbital period and eccentricity for the surviving BH binary of the PTB after undergoing an SNe event. The darker the color, the higher the probability. The red and green markers represent the locations of the PTB before the SNe and the observed location of G3425, respectively. The left and right panels show the Maxwellian distributions for σ_k values of 50 and 10 km s^{-1}, respectively.

expect it to result in a smaller required $\Delta E_{\rm orb,out}$ for ejecting the CE, and the $a_{\rm out}$ after ejecting CE will be larger. In Figure 1, the merger product of the inner binary, along with the successfully ejected core of the donor, forms a PTB with an orbital separation (orbital period) of 687 $R_\odot$ (547 days) and an eccentricity of 0. We find that this result is very similar to the simulations by H. Glanz & H. B. Perets (2021). Compared to a traditional binary common envelope (BCE), in TCE, the $E_{\rm orb}$ is generated by the inspiral of the inner binary due to friction as an additional energy source transferred to CE. This accelerates the expansion and ejection of CE, thereby reducing the dissipation of $E_{\rm orb,out}$ and the inspiral of the outer orbit. This means that, without increasing $\alpha_{\rm ce}$, TCE is more likely than BCE to produce binaries with long $P_{\rm orb}$.

Additionally, Figure 3 shows the distribution of the initial masses of the three stars, the initial inner and outer orbital periods, and the orbital period of the PTBs ($P_{\rm orb,PTB}$) under the assumption that $\alpha_{\rm CE,in} = \alpha_{\rm CE,out} = 1$. In our TCE model, the $E_{\rm bind}$ of ejecting the tertiary is mainly provided by $\Delta E_{\rm orb,in}$, which is primarily determined by $\frac{m_{1,\rm ini} m_{2,\rm ini}}{m_{1,\rm ini}+m_{2,\rm ini}}$ (see Equation (3)). The larger $\frac{m_{1,\rm ini} m_{2,\rm ini}}{m_{1,\rm ini}+m_{2,\rm ini}}$ is, the greater the $\Delta E_{\rm orb,in}$, which ultimately increases the likelihood of forming PTBs with longer orbital periods (see Figure 3). In addition, the larger $m_{3,\rm ini}$, the greater its mass-loss rate (J. S. Vink et al. 2001). This results in a smaller envelope mass and a larger $a_{\rm out}$ at the time of TCE and ultimately a smaller $E_{\rm bind}$ during the TCE process. This also increases the likelihood of forming PTBs with longer orbital periods (see the left panel of Figure 3). On the other hand, $\Delta E_{\rm orb,in}$ and $\Delta E_{\rm orb,out}$ are mainly determined by the final orbital energy ($E_{\rm orb,in,f}$ and $E_{\rm orb,out,f}$), because the $a_{\rm in,i}$ and $a_{\rm out,i}$ are very large, and its $E_{\rm orb,in,i}$ and $E_{\rm orb,out,i}$ can be almost neglected (see Equation (3)). This ultimately leads to a weak correlation between the size of the $P_{\rm orb,PTB}$ and $P_{\rm in,ini}$, $P_{\rm out,ini}$ (see the middle and right panels of Figure 3). Most of $P_{\rm orb,PTB}$ range from 10 to 100 days, followed by 100 to 1000 days, with only a very few $P_{\rm orb,PTB}$ greater than 1000 days (in our calculation, the maximum $P_{\rm orb,PTB}$ is ∼1850 days). We estimate that the $P_{\rm orb,PTB}$ is 1–2 orders of magnitude larger than those of the binaries formed through BCE evolution (under the same $\alpha_{\rm CE}$ assumption).

In Figure 1, we use the binary module with a metallicity of $Z = 0.014$ of MESA to further track the evolution of PTB. Due to the strong Wolf–Rayet winds (at a mass-loss rate of $\sim 10^{-5.5}\, M_\odot\, {\rm yr}^{-1}$), $P_{\rm orb}$ widens to 745 days. Around 10.2 Myr, the helium star's core depletes carbon, at which point it is assumed to undergo an SN. Additionally, at the time of SN, the helium star has a mass of 6.21 $M_\odot$, with an $M_{\rm CO}$ of 4.21 $M_\odot$.

Using Equations (4) and (5), we calculate the $P_{\rm BH} = \frac{4.21-2}{5} \cong$ 44.2% and the $P_{\rm CF} = \frac{4.21-2}{6} \cong$ 36.8% in the SNe event. It is worth noting that, as described in Section 2.2, if the BH is formed through a CF process, in our model, the resulting BH mass would be equal to the helium star mass (∼6.21 $M_\odot$), which does not match the BH mass of G3425. In our calculation, the probability of forming a BH through this non-CF process is $P = P_{\rm BH}(1 - P_{\rm CF}) \cong 27.9\%$. We also calculate that in the case of non-CF, the remnant mass distribution follows a normal distribution with a mean of 3.37 $M_\odot$ and a standard deviation of 0.5 $M_\odot$. The BH mass in G3425 (∼3.6 $M_\odot$) falls within one standard deviation from the mean of this normal distribution. Figure 4 shows the probability distribution of the post-SN surviving BH binary orbits for the systems selected in Figure 1

under different σ_k values for the Maxwellian distribution. Since $\sigma_k = 50\,\mathrm{km\,s^{-1}}$ is larger than $\sigma_k = 10\,\mathrm{km\,s^{-1}}$, the PTB typically receives a greater natal kick, resulting in a more dispersed orbital probability distribution and a lower survival rate for the PTB (survival rates of 8.5% and 36.9% for the left and right panels, respectively). In the Figure 4, by comparing with the observed orbital properties of G3425, we find that G3425 lies in the highest-probability region (black area) of the surviving post-SNe BH binary orbit distribution, and the natal kicks required to form G3425 are approximately 49^{+39}_{-39} and 11^{+16}_{-5} $\mathrm{km\,s^{-1}}$, respectively. However, we find that forming G3425 from this SNe event remains quite challenging, as there is still a significant probability (∼55.8%) that the helium star would form an NS during the SNe event. Additionally, it is necessary to avoid forming a BH through CF, and finally, the PTB needs to avoid being disrupted during the SNe event. This conclusion is very similar to the simulation results by S. Wang et al. (2024).

In Figure 1, we select a post-SN BH binary orbit that is closest to G3425 and continue to track its evolution. At ∼559 Myr, the merger product of the inner binary leaves MS and enters the RG phase, indicating that the binary reaches the G3425 stage. The G3425 phase lasts for about 161.8 Myr. At around 720.9 Myr, the RG star fills its Roche lobe, marking the end of the G3425 phase and the beginning of the LMXB phase. During the MT process, the mass of the donor is less than that of the accretor, causing the separation to gradually widen and the Roche lobe radius to increase. Additionally, due to mass loss from the RG and the BH being constrained by the Eddington accretion rate, approximately $0.92\,M_\odot$ of mass is lost from the system during the MT process. When the Roche lobe radius becomes greater than the radius of the donor, MT stops. At this point, the $P_{\rm orb}$ is 1733 days, with the mass of $M_{\rm BH}$ being $4.38\,M_\odot$ and the RG having a mass of $0.77\,M_\odot$. The LMXB phase lasts approximately 1.12 Myr, during which the mass accretion rate of the BH ($\sim 6.69 \times 10^{-7}\,M_\odot\,\mathrm{yr^{-1}}$) is about 20 times higher than the Eddington accretion rate. Therefore, this LMXB phase is likely to be an ultraluminous X-ray source (K. Abdusalam et al. 2020). In the subsequent evolution, the RG cools and forms a $0.76\,M_\odot$ carbon–oxygen white dwarf, resulting in a final $P_{\rm orb}$ of 1732.23 days, making it impossible for the system to merge within a Hubble time.

4. Conclusion

Using the MSE and MESA codes, we discuss that G3425 originated from a triple and evolved through a TCE. Based on the results of the 3D simulations of TCE by H. Glanz & H. B. Perets (2021), we estimate the possible outcomes of TCE using the standard energy formalism on a 1D scale. We find that when the inner binary merges during the TCE process due to inspiral, the resulting $\Delta E_{\rm orb,in}$ contributes a significant proportion of $E_{\rm bind}$, approximately 97% in our simulations. This means that, during TCE, the outer orbit does not need to supply much $\Delta E_{\rm orb,out}$ to successfully eject CE. Therefore, in our simulations, the final outcome of TCE is the merger of the inner binary, the successful ejection of the donor's core, and an ejected orbital separation that is 1–2 orders of magnitude larger than that of a classical BCE with successful ejection. The result of this simulation is very similar to that of H. Glanz & H. B. Perets (2021), despite our modeling being conducted on a 1D scale. It is worth noting that in our TCE simulation, we did not increase the $\alpha_{\rm CE}$, instead using $\alpha_{\rm CE} = 1$. Subsequently, in the SNe simulations, we find that it is still challenging for the ejected helium star to form G3425, even though the observed G3425 falls within the highest-probability region of the surviving post-SNe BH binary orbital distribution in our simulations. The reason is that this helium star not only has a significant probability (∼55.8%) of forming an NS after the SNe but also needs to avoid forming a BH through CF. Finally, the PTB must survive during the SNe event, with survival rates of 8.5% and 36.9% for σ_k of 50 and $10\,\mathrm{km\,s^{-1}}$, respectively. This could potentially explain why BHs in the mass gap are so rare. Additionally, in cases where σ_k is 50 and $10\,\mathrm{km\,s^{-1}}$, the natal kicks required to form G3425 are 49^{+39}_{-39} and 11^{+16}_{-5} $\mathrm{km\,s^{-1}}$, respectively. Combined with the calculated survival rates, these results suggest that the formation of G3425 is more likely to occur with a low natal kick.

Acknowledgments

This work received the support of the National Natural Science Foundation of China under grants U2031204, 12163005, 12373038, and 12288102; the Natural Science Foundation of Xinjiang No. 2022TSYCLJ0006 and 2022D01D85; and the science research grants from the China Manned Space Project No. CMS-CSST-2021-A10.

ORCID iDs

Zhuowen Li https://orcid.org/0009-0006-1716-357X
Xizhen Lu https://orcid.org/0000-0002-3849-8962
Guoliang Lü https://orcid.org/0000-0002-3839-4864
Chunhua Zhu https://orcid.org/0000-0003-4589-1241
Jinlong Yu https://orcid.org/0000-0001-8493-5206

References

Abdusalam, K., Ablimit, I., Hashim, P., et al. 2020, ApJ, 902, 125
Anderson, K. R., Lai, D., & Storch, N. I. 2017, MNRAS, 467, 3066
Andrews, J. J., & Kalogera, V. 2022, ApJ, 930, 159
Antonini, F., Toonen, S., & Hamers, A. S. 2017, ApJ, 841, 77
Bailyn, C. D., Jain, R. K., Coppi, P., & Orosz, J. A. 1997, AAS Meeting Abstracts, 190, 10.01
Belczynski, K., & Ziolkowski, J. 2009, ApJ, 707, 870
Blaes, O., Lee, M. H., & Socrates, A. 2002, ApJ, 578, 775
Brott, I., de Mink, S. E., Cantiello, M., et al. 2011, A&A, 530, A115
Bruenech, C. W., Boekholt, T., Kummer, F., & Toonen, S. 2025, A&A, 693, A14
Burdge, K. B., El-Badry, K., Kara, E., et al. 2024, Natur, 635, 316
Burrows, A., Vartanyan, D., & Wang, T. 2023, ApJ, 957, 68
Casares, J., & Jonker, P. G. 2014, SSRv, 183, 223
Chakrabarti, S., Simon, J. D., Craig, P. A., et al. 2023, AJ, 166, 6
Chawla, C., Chatterjee, S., Breivik, K., et al. 2022, ApJ, 931, 107
Chawla, C., Chatterjee, S., Shah, N., & Breivik, K. 2024, ApJ, 975, 163
Coleman, M. S. B., & Burrows, A. 2022, MNRAS, 517, 3938
Comerford, T. A. F., & Izzard, R. G. 2020, MNRAS, 498, 2957
Corral-Santana, J. M., Casares, J., Muñoz-Darias, T., et al. 2016, A&A, 587, A61
De, K., MacLeod, M., Jencson, J. E., et al. 2024, arXiv:2410.14778
de Vries, N., Portegies Zwart, S., & Figueira, J. 2014, MNRAS, 438, 1909
Dorozsmai, A., Toonen, S., Vigna-Gómez, A., de Mink, S. E., & Kummer, F. 2024, MNRAS, 527, 9782
Eggleton, P. P. 1983, ApJ, 268, 368
Eggleton, P. P., & Kiseleva-Eggleton, L. 2001, ApJ, 562, 1012
Ekström, S., Georgy, C., Eggenberger, P., et al. 2012, A&A, 537, A146
El-Badry, K., Rix, H.-W., Cendes, Y., et al. 2023a, MNRAS, 521, 4323
El-Badry, K., Rix, H.-W., Quataert, E., et al. 2023b, MNRAS, 518, 1057
Eldridge, J. J., Stanway, E. R., Xiao, L., et al. 2017, PASA, 34, e058
Farr, W. M., Sravan, N., Cantrell, A., et al. 2011, ApJ, 741, 103
Fragos, T., Andrews, J. J., Bavera, S. S., et al. 2023, ApJS, 264, 45
Fryer, C. L., Belczynski, K., Wiktorowicz, G., et al. 2012, ApJ, 749, 91
Fryer, C. L., & Kalogera, V. 2001, ApJ, 554, 548
Gaia Collaboration, Panuzzo, P., Mazeh, T., et al. 2024, A&A, 686, L2

Giacobbo, N., Mapelli, M., & Spera, M. 2018, MNRAS, 474, 2959
Gilkis, A., & Mazeh, T. 2024, MNRAS, 535, L44
Glanz, H., & Perets, H. B. 2021, MNRAS, 500, 1921
Hamers, A. S. 2018, MNRAS, 476, 4139
Hamers, A. S. 2020, MNRAS, 494, 5492
Hamers, A. S., Glanz, H., & Neunteufel, P. 2022a, ApJS, 259, 25
Hamers, A. S., Perets, H. B., Thompson, T. A., & Neunteufel, P. 2022b, ApJ, 925, 178
Hamers, A. S., & Portegies Zwart, S. F. 2016, MNRAS, 459, 2827
Hamers, A. S., Rantala, A., Neunteufel, P., Preece, H., & Vynatheya, P. 2021, MNRAS, 502, 4479
Holman, M., Touma, J., & Tremaine, S. 1997, Natur, 386, 254
Hurley, J. R., Pols, O. R., & Tout, C. A. 2000, MNRAS, 315, 543
Hurley, J. R., Tout, C. A., & Pols, O. R. 2002, MNRAS, 329, 897
Iben, I., J., & Livio, M. 1993, PASP, 105, 1373
Ivanova, N., Justham, S., Chen, X., et al. 2013, A&ARv, 21, 59
Ivanova, N., Justham, S., & Ricker, P. 2020, Common Envelope Evolution,
Janka, H.-T., & Kresse, D. 2024, Ap&SS, 369, 80
Kimball, C., Imperato, S., Kalogera, V., et al. 2023, ApJL, 952, L34
Kippenhahn, R., & Weigert, A. 1994, Stellar Structure and Evolution (Berlin: Springer),
Kotko, I., Banerjee, S., & Belczynski, K. 2024, MNRAS, 535, 3577
Kozai, Y. 1962, AJ, 67, 591
Kruckow, M. U., Andrews, J. J., Fragos, T., et al. 2024, A&A, 692, A141
Kruckow, M. U., Tauris, T. M., Langer, N., Kramer, M., & Izzard, R. G. 2018, MNRAS, 481, 1908
Kummer, F., Toonen, S., Dorozsmai, A., Grishin, E., & de Koter, A. 2025, A&A, 693, A84
Langer, N. 1991, A&A, 252, 669
Li, Z., Zhu, C., Lü, G., et al. 2024a, ApJ, 969, 160
Li, Z., Zhu, C., Lu, X., et al. 2024b, ApJL, 975, L8
Lidov, M. L. 1962, P&SS, 9, 719
Livio, M., & Soker, N. 1988, ApJ, 329, 764
Loveridge, A. J., van der Sluys, M. V., & Kalogera, V. 2011, ApJ, 743, 49
Lu, X., Zhu, C., Liu, H., et al. 2023, A&A, 674, A216
Mandel, I., & Müller, B. 2020, MNRAS, 499, 3214
Mapelli, M., & Giacobbo, N. 2018, MNRAS, 479, 4391
Mardling, R. A., & Aarseth, S. J. 2001, MNRAS, 321, 398
Martinez, M. A. S., Fragione, G., Kremer, K., et al. 2020, ApJ, 903, 67
Mata Sanchez, D., Torres, M. A. P., Casares, J., et al. 2024, arXiv:2408.13310
McClintock, J. E., & Remillard, R. A. 2006, in Compact Stellar X-ray Sources, ed. W. H. G. Lewin & M. van der Klis, 39 (Cambridge: Cambridge Univ. Press), 157
Mirabel, I. F., & Rodrigues, I. 2003, Sci, 300, 1119
Moe, M., & Di Stefano, R. 2017, ApJS, 230, 15
Müller, B., Heger, A., Liptai, D., & Cameron, J. B. 2016, MNRAS, 460, 742
Nagarajan, P., & El-Badry, K. 2024, arXiv:2411.16847
Naoz, S. 2016, ARA&A, 54, 441
Naoz, S., & Fabrycky, D. C. 2014, ApJ, 793, 137
Naoz, S., Fragos, T., Geller, A., Stephan, A. P., & Rasio, F. A. 2016, ApJL, 822, L24
Nugis, T., & Lamers, H. J. G. L. M. 2000, A&A, 360, 227
Özel, F., Psaltis, D., Narayan, R., & McClintock, J. E. 2010, ApJ, 725, 1918
Paczynski, B. 1976, in IAU Symp. Vol. 73, Structure and Evolution of Close Binary Systems, ed. P. Eggleton, S. Mitton, & J. Whelan (Dordrecht: Reidel), 75
Pauli, D., Langer, N., Aguilera-Dena, D. R., Wang, C., & Marchant, P. 2022, A&A, 667, A58
Paxton, B., Bildsten, L., Dotter, A., et al. 2011, ApJS, 192, 3
Paxton, B., Cantiello, M., Arras, P., et al. 2013, ApJS, 208, 4
Paxton, B., Marchant, P., Schwab, J., et al. 2015, ApJS, 220, 15
Paxton, B., Schwab, J., Bauer, E. B., et al. 2018, ApJS, 234, 34
Paxton, B., Smolec, R., Schwab, J., et al. 2019, ApJS, 243, 10
Podsiadlowski, P., Cannon, R. C., & Rees, M. J. 1995, MNRAS, 274, 485
Qin, Y., Hu, R. C., Meynet, G., et al. 2023, A&A, 671, A62
Rajamuthukumar, A. S., Hamers, A. S., Neunteufel, P., Pakmor, R., & de Mink, S. E. 2023, ApJ, 950, 9
Rantala, A., Pihajoki, P., Mannerkoski, M., Johansson, P. H., & Naab, T. 2020, MNRAS, 492, 4131
Remillard, R. A., & McClintock, J. E. 2006, ARA&A, 44, 49
Riley, J., Agrawal, P., Barrett, J. W., et al. 2022, ApJS, 258, 34
Röpke, F. K., & De Marco, O. 2023, LRCA, 9, 2
Rostami-Shirazi, A., Hasani Zonoozi, A., Haghi, H., & Rabiee, M. 2024, MNRAS, 535, 3489
Sabach, E., & Soker, N. 2015, MNRAS, 450, 1716
Salas, J. M., Naoz, S., Morris, M. R., & Stephan, A. P. 2019, MNRAS, 487, 3029
Sana, H., de Koter, A., de Mink, S. E., et al. 2013, A&A, 550, A107
Schneider, F. R. N., Podsiadlowski, P., & Müller, B. 2021, A&A, 645, A5
Shao, Y., & Li, X.-D. 2015, ApJ, 809, 99
Shao, Y., & Li, X.-D. 2020, ApJ, 898, 143
Shao, Y., & Li, X.-D. 2021, ApJ, 920, 81
Shariat, C., Naoz, S., El-Badry, K., et al. 2024, arXiv:2411.15644
Shariat, C., Naoz, S., El-Badry, K., et al. 2025, ApJ, 978, 47
Shariat, C., Naoz, S., Hansen, B. M. S., et al. 2023, ApJL, 955, L14
Shenar, T., Sana, H., Mahy, L., et al. 2022, NatAs, 6, 1085
Soker, N. 2021, MNRAS, 504, 5967
Stegmann, J., Antonini, F., & Moe, M. 2022, MNRAS, 516, 1406
Sukhbold, T., Ertl, T., Woosley, S. E., Brown, J. M., & Janka, H. T. 2016, ApJ, 821, 38
Tanikawa, A., Hattori, K., Kawanaka, N., et al. 2023, ApJ, 946, 79
Toonen, S., Hamers, A., & Portegies Zwart, S. 2016, ComAC, 3, 6
Toonen, S., Perets, H. B., & Hamers, A. S. 2018a, A&A, 610, A22
Toonen, S., Perets, H. B., Igoshev, A. P., Michaely, E., & Zenati, Y. 2018b, A&A, 619, A53
Toonen, S., Portegies Zwart, S., Hamers, A. S., & Bandopadhyay, D. 2020, A&A, 640, A16
Tout, C. A., Aarseth, S. J., Pols, O. R., & Eggleton, P. P. 1997, MNRAS, 291, 732
van den Heuvel, E. P. J. 1976, in IAU Symp. Vol. 73, Structure and Evolution of Close Binary Systems, ed. P. Eggleton, S. Mitton, & J. Whelan, 35
Vetter, M., Röpke, F. K., Schneider, F. R. N., et al. 2024, A&A, 691, A244
Vigna-Gómez, A., Willcox, R., Tamborra, I., et al. 2024, PhRvL, 132, 191403
Vink, J. S., de Koter, A., & Lamers, H. J. G. L. M. 2001, A&A, 369, 574
von Zeipel, H. 1910, AN, 183, 345
Walk, L., Tamborra, I., Janka, H.-T., Summa, A., & Kresse, D. 2020, PhRvD, 101, 123013
Wang, S., Zhao, X., Feng, F., et al. 2024, NatAs, 8, 1583
Webbink, R. F. 1984, ApJ, 277, 355
Xu, X.-J., & Li, X.-D. 2010, ApJ, 716, 114
Zorotovic, M., Schreiber, M. R., Gänsicke, B. T., & Nebot Gómez-Morán, A. 2010, A&A, 520, A86